# Introduction to ultra-short pulses

## 2.1 Introduction

I start this chapter by giving an introduction to the basic concepts relative to ultra-short pulses. In particular I define the concepts of temporal contrast and Carrier Envelope Phase that are fundamental to understand the work presented in this manuscript. I then introduce the main techniques for the temporal characterization of ultra-short pulses such as second order autocorrelation, SPIDER and FROG. I also introduce a new pulse characterization device (Phazzler) that combines, in a same instrument, all these characterization techniques. I conclude this chapter by presenting the third order correlation technique that is used to characterize the pulses with a high temporal dynamic range.

## 2.2 Ultra-short laser pulses

The electric field of a linearly polarized optic wave is a real function varying with time, solution of the Maxwell equations. This function $\mathcal{E}(t)$ can be decomposed into frequencies by making a Fourier transform to obtain:

$$\tilde{\mathcal{E}}(\omega) = \int_{-\infty}^{+\infty} \mathcal{E}(t) exp(i\omega t) dt. \tag{2.1}$$

A complex temporal analytic signal can also be defined as:

$$E(t) = 2 \int_{0}^{+\infty} \tilde{\mathcal{E}}(\omega) exp(-i\omega t) \frac{d\omega}{2\pi}, \tag{2.2}$$

with an associated Fourier transform spectral decomposition:

$$\tilde{E}(\omega) = \int_{-\infty}^{+\infty} E(t) exp(i\omega t) dt = \left|\tilde{E}(\omega)\right| exp(i\varphi(\omega)) \tag{2.3}$$

This field is zero for negative frequencies and equal to $2\tilde{\mathcal{E}}(\omega)$ for positive frequencies. The basic idea behind working with analytic signals is that the negative frequency components of the

Fourier transform (or spectrum) of a real-valued function are superfluous, due to the Hermitian symmetry of such a spectrum. They can be discarded with no loss of actual information. The quantity $I(\omega) = \frac{\epsilon_0 c}{2}\left|\tilde{E}(\omega)\right|^2$ is the spectral intensity and $\varphi(\omega)$ is the spectral phase. The spectral phase is typically expanded in a Taylor series around the central frequency $\omega_0$:

$$\varphi(\omega) = \sum_{k=0}^{n} \frac{\varphi^{(k)}}{k!}(\omega - \omega_0)^k \tag{2.4}$$

Where $\varphi^{(2)}$ is the linear chirp (also named Group Delay Dispersion GDD or second-order phase dispersion) and $\varphi^{(3)}$ the quadratic chirp. In the temporal domain a temporal phase $\varphi(t)$ is also defined and the complex temporal field is written as: $E(t) = |E(t)|\, exp(i(\varphi_0 + \varphi(t) - \omega_0 t))$. $|E(t)|$ is the temporal envelope. Assuming $\varphi(0) = 0$, $\varphi_0$ is the phase shift between the electric field and the envelope. This term is also called carrier envelope phase (CEP). $I(t) \propto |E(t)|^2$ is the cycle-averaged radiation intensity. For a Gaussian pulse the intensity is $I(t) = E_0 exp\left(\frac{-2t^2}{\tau^2}\right)$ with $\tau$ the width at $1/e^2$ in intensity. The Full Width at Half Maximum (FWHM) in intensity, $\Delta t$, is related to $\tau$ by: $\Delta t = \tau\sqrt{2ln(2)}$. Fig. 2.1 shows the electric field (red) and the envelope (blue) for two pulses having a FWHM of 25 fs and 5 fs at a central wavelength of 800 nm. Pulses as short as 5 fs contain just 3 optical cycles at $\lambda = 800nm$.

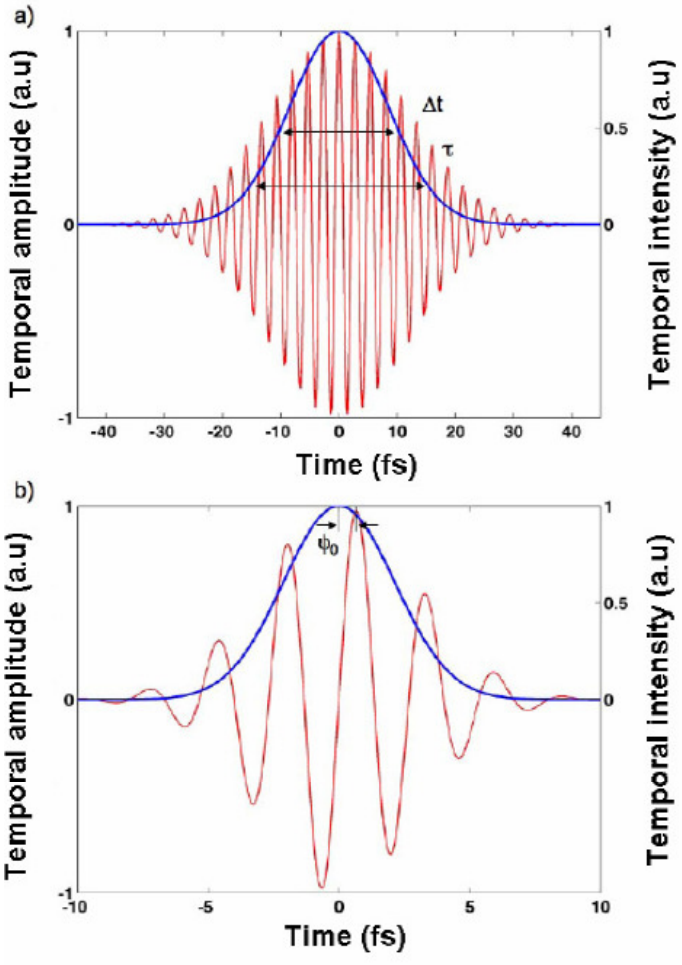


Figure 2.1: Electric field (red) and associated temporal intensity (blue) for pulses with a FWHM of: 25 fs (a) and 5 fs (b)

### 2.2.1 CEP and its stabilization

A more detailed description of the CEP measurement and stabilization in a laser system with a fast and a slow feedback loop is given with the description of the development of the laser source (chapter 6). Here I just want to derive the CEP off-set between successive output pulses of an oscillator and how to stabilize it. Inside the laser cavity, together with the Ti:sapphire crystal, there are other dispersive elements. All together they are responsible for the variation of the off-set between the carrier wave and the envelope of the pulses. This variation is caused by the difference between the phase velocity $v_f = \frac{\omega}{k_0}$ (where $k_0 = 2\pi/\lambda$ is the constant of propagation) of the carrier wave and the group velocity $v_g = \frac{\partial\omega}{\partial k_0}$ of the pulse envelope. In dispersive media the group and phase velocity are different and there is a shift between the envelope and the carrier inside the cavity. The consequence is that the CEP varies between successive pulses at the output of the oscillator. Without any perturbation the CEP, $\varphi_0$, varies by a fixed quantity $\Delta\varphi_0$ between two successive pulses. This phase difference contains typically some hundreds of times $2\pi$, plus a significant term between 0 and $2\pi$. This value is defined $\Delta\varphi_0$ [1]. Considering a cavity length L, $\Delta\varphi_0$ is given by the expression:

$$\Delta\varphi_0 = 2\pi \int_0^{2L} \frac{dn(z)}{d\lambda_0} dz \tag{2.5}$$

where n(z) is the index of refraction of the materials inside the cavity. In reality $\varphi_0$ varies between successive pulses by the quantity $\Delta\varphi_0$ plus a random variation due to perturbations of the laser cavity and fluctuations of the energy of the pump pulses.
The variation of the CEP, $\Delta\varphi_0$, is the quantity that can be experimentally measured and used for the stabilization. The stabilization is realized in frequency domain. In frequency domain, the frequency comb of the oscillator is shifted compared to the repetition frequency, $f_{rep}$, by an offset frequency, $f_{ceo}$, which is a direct function of $\Delta\varphi_0$ (Fig. 2.2). The value of $f_{ceo}$ is given by the relation:

$$f_{ceo} = (\Delta\varphi_0/2\pi) f_{rep} \tag{2.6}$$

Measuring $f_{ceo}$ and making it constant implies that successive pulses of the cavity have a fixed $\Delta\varphi_0$. A self-referenced interferometer for measuring $f_{ceo}$ is presented in section 6.2.1

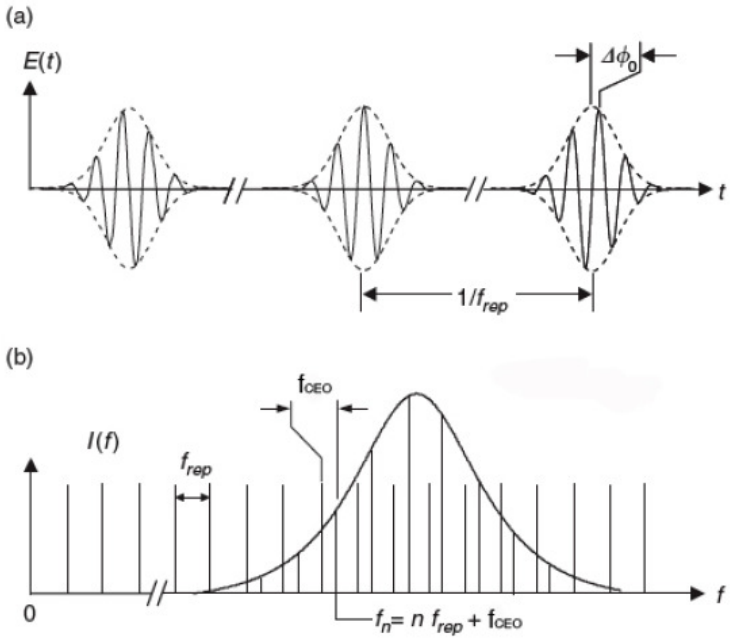


Figure 2.2: Correspondence between the temporal and frequency domain. (a) In the temporal domain $\varphi_0$ varies by a quantity $\Delta\varphi_0$. (b) In the frequency domain there is a frequency comb with a frequency $f_{rep}$. This comb is translated by the integer multiple frequencies by an offset $f_{ceo}$. Its amplitude is given by the Fourier transform of the temporal amplitude of the pulse at $\omega_0$. Reprinted from [1]

### 2.2.2 Temporal contrast of a short pulse

Every process of amplification introduces a certain amount of noise on the amplified signal and causes some distortion. This is true for electronic amplification and it is also verified for optical amplification. For ultra-intense sources, the temporal quality of the pulses and, in particular, the ratio between the peak intensity and the intensity at a delay $\Delta t$, is defined as the temporal contrast of the pulses at this delay. This quantity has a fundamental importance in laser-matter interaction. Focusing a 25 fs pulse with an energy $> 1$ mJ in a spot size of 1 $\mu m$ (limit of diffraction at 800 nm) produces a peak intensity higher than $10^{18} W/cm^2$. With a temporal contrast of 6 orders of magnitude the intensity of the background pedestal, $\approx 10^{12} W/cm^2$, is high enough to pre-ionize the target (for example fused silica) before the arrival of the main, ultra-short pulse [15]. If the plasma is generated before the main pulse arrives, it will expand hydrodynamically and the main pulse will no longer interact with a clean, steep plasma density. This deformation of the plasma-vacuum interface has a strong influence on processes such as high-order harmonic generation from solid surfaces [17] and ion acceleration [7]. To better understand the concept of contrast Fig. 2.3 shows, on logarithmic scale, the typical temporal profile of a short pulse. Four types of contributions can be distinguished:

- A long pedestal (>100ps);
- A short pedestal (some tens of time the pulse duration);

- pre-pulses: replicas situated in front of the pulse

- post-pulses: replicas situated after the pulse.

These structures have different physical origins. The long pedestal corresponds to the incoherent noise introduced by the amplified spontaneous emission (ASE) and for this reason it is called incoherent contrast. The ASE is mainly generated in the first, high gain, amplification stages. The short pedestal comes from an imperfect recompression after the stretcher/compressor and amplification and is called the coherent contrast. Finally pre-pulses and post-pulses are replicas of the main pulse due to reflection or diffusion from optical surfaces and from non linear effects such as four-wave mixing [9].

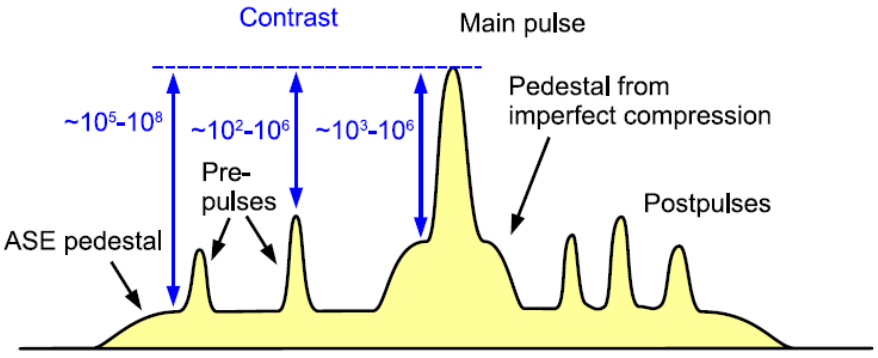


Figure 2.3: Typical temporal profile of the output pulse of a (CPA) laser. Aside from the main pulse, it generally has pre- and post-pulses. The underlying pedestal comes from ASE (ns) and imperfect compression (ps). Reprinted from [12]

## 2.3 Temporal characterization of femtosecond pulses

This section presents a brief review of the main solutions for the temporal characterization of femtosecond pulses. As discussed in the previous section, imperfections in the temporal compression influence not only the temporal width of the pulse but also affect its coherent contrast. During my Ph.D I contributed to the development of a temporal characterization device named Phazzler (Fastlite) that makes it possible to carry out several temporal characterization techniques using the same instrument. A presentation of this device is given at the end of this section.

### 2.3.1 Second order autocorrelator

One of the first techniques for the temporal characterization of femtosecond pulses is the second order autocorrelation [2]. For some particular temporal profiles, the FWHM of the temporal intensity and of the autocorrelation are linked. With an assumption of the temporal profile, the corresponding FWHM is retrieved measuring the FWHM of the second order autocorrelation. A schematic of this device is shown in Fig. 2.5. The input pulse is split into two temporally delayed replicas in a Michelson interferometer and the two replicas are focused into a non linear crystal. The signal is detected with a photodiode or a photomultiplier and visualized with an oscilloscope. The result of the nonlinear interaction of the beams from the two arms depends on the delay. This signal is named autocorrelation function. There are two types of autocorrelations:

- Interferometric autocorrelation: when the beams incident on the crystal are collinear (can not be distinguished).
- Intensity autocorrelation: for non collinear beams.

#### Interferometric autocorrelator

For the interferometric autocorrelator the measured signal is given by the expression:

$$S_{col}(\tau) \propto \int_{-\infty}^{+\infty} \left|(E(t) + E(t-\tau))^2\right|^2 dt \tag{2.7}$$

where $\tau$ is the delay between the pulses. This signal is the sum of three components function of $\tau$: $S_{col}(\tau) \propto I_{back} + I_{int}(\tau) + I_{\omega}(\tau) + I_{2\omega}(\tau)$ with:

$$I_{back} = \int_{-\infty}^{\infty} (|E(t-\tau)|^4 + |E(t)|^4) dt = 2\int_{-\infty}^{\infty} I^2(t) dt \tag{2.8}$$

$$I_{int}(\tau) = 4\int_{-\infty}^{\infty} (|E(t-\tau)|^2 |E(t)|^2 = 4\int_{-\infty}^{\infty} I(t-\tau) I(\tau) dt \tag{2.9}$$

$$I_{\omega}(\tau) = 4\int_{-\infty}^{\infty} Re[(I(t) + I(t-\tau))E^*(t)E(t-\tau)exp(i\omega_0\tau)]dt, \tag{2.10}$$

$$I_{2\omega}(\tau) = 2\int_{-\infty}^{\infty} Re[(E(t)^2(E^*(t-\tau))^2 exp(i2\omega_0\tau)]dt \tag{2.11}$$

$I_{back}$ is a background signal independent of $\tau$, $I_{int}(\tau)$ is the intensity autocorrelation, $I_{\omega}(\tau)$ and $I_{2\omega}(\tau)$ are named coherence term oscillating respectively at $\omega_0$ and $2\omega_0$. There is a ratio 8 between the maximum ($\tau = 0$) and the minimum signal. When the delay is large enough to avoid temporal overlap between the pulses the measured signal is twice the one measured with a single beam. When the delay is zero the signal is equal to $2^4 = 16$. The ratio between the two is then equal to 8. An example of an interferometric trace is shown in Fig. 2.5. Even if there are algorithms for extracting the spectral phase from an interferometric trace, for example PICASO, (Phase and Intensity from Cross Correlation and Spectrum Only) this reconstruction is not robust and does not always converge.

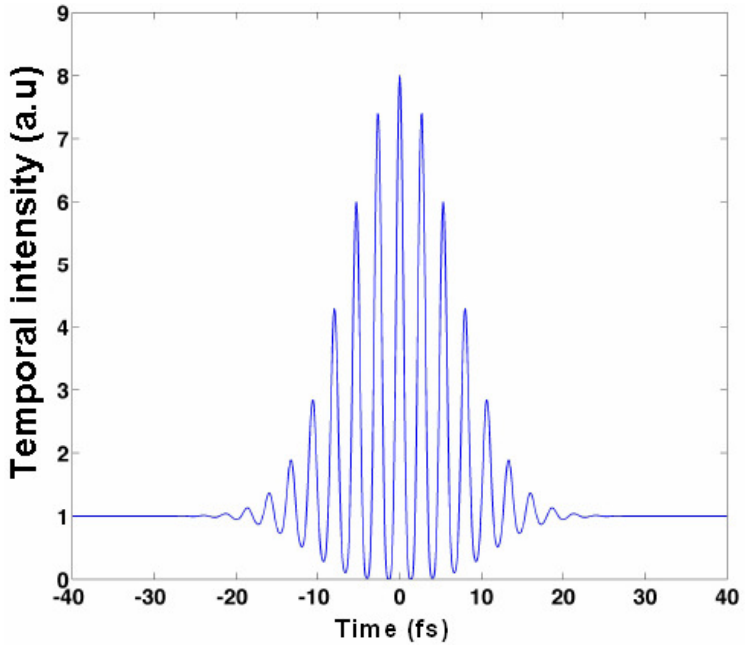


Figure 2.4: Calculated interferometric autocorrelation for a 10 fs pulse

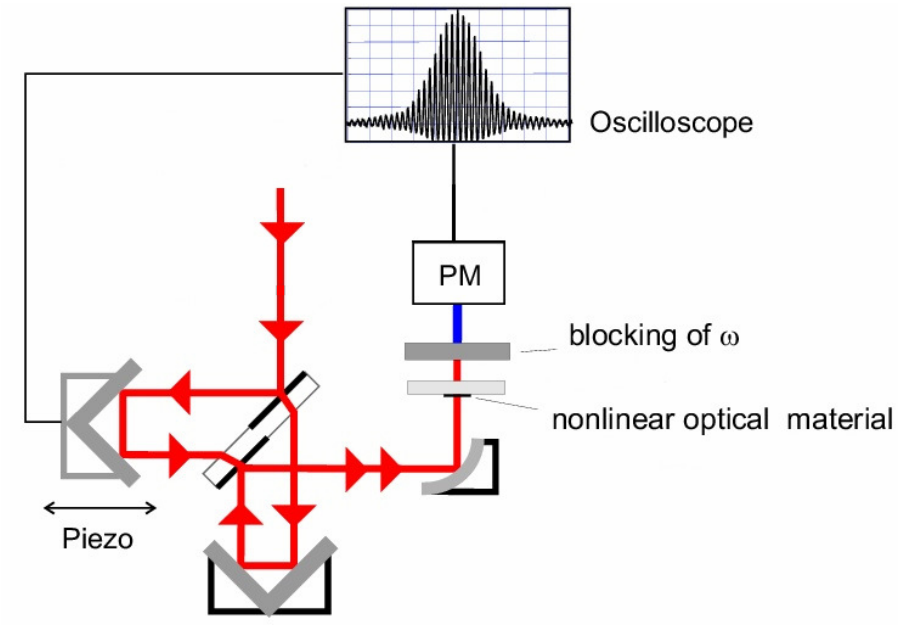


Figure 2.5: Schematic of a second order autocorrelator. The detector can be a photomultiplier (MHz detection) or a photodiode (kHz detection). Reprinted from [4]

### Intensity autocorrelator

For the intensity autocorrelator the measured signal is given by the expression:

$$S_{non-col}(\tau) = I_{int}(\tau) \propto \int_{-\infty}^{+\infty} |E(t)E(t-\tau)|^2 \, dt = \int_{-\infty}^{+\infty} I(t)I(t-\tau)dt \tag{2.12}$$

The signal is measured in the direction corresponding to the addition of the wave vectors of the two arms. The intensity autocorrelation does not contain full information about

the electric field of the pulse, since the phase of the pulse in the time domain is completely lost. The only information that can retrieved is the FWHM and basic shape of the input pulses.

Two main techniques have been developed to measure the spectral phase of femtosecond pulses: SPIDER and FROG.

### 2.3.2 SPIDER technique

Spectral Phase Interferometry for Direct Electric-field Reconstruction (SPIDER) [6, 5] uses spectral shearing interferometry to retrieve the spectral phase of an incident pulse. This form of interferometry measures the interference between two pulses separated in time which are identical except for their central frequencies. This pulse pair is said to be spectrally sheared. Nonlinear optics provides a general approach to globally shearing two pulses by a frequency $\Omega$. This can be done by sum frequency generation between a monochromatic frequency, $\Omega$, and the field we want to shear, $\tilde{E}(\omega)$, resulting in a sheared field, $\tilde{E}(\omega+\Omega)$. It is convenient to obtain the monochromatic frequency from a strongly chirped ultrashort pulse for which the instantaneous frequency, which is approximately a linear function of time, does not vary during the nonlinear interaction with the short pulse(Fig. 2.6). The magnitude of the spectral shear generated in this manner is then a function of two parameters: the delay between the pulses and the amount of chirp of the stretched pulse. The exact value of the shear is equal to: $\Omega = -\frac{\tau}{2\varphi_2}$ where $\tau$ is the delay between the pulses and $\varphi_2$ is the second order dispersion present on the chirped pulse.

The interference of the two sheared pulses (SPIDER signal) is given by:

$$I_{SPIDER}(\omega) = \left|\tilde{E}(\omega)\right|^2 + \left|\tilde{E}(\omega+\delta\omega)\right|^2 + 2\left|\tilde{E}(\omega)\tilde{E}(\omega+\delta\omega)\right| \times cos(\phi(\omega+\delta\omega) - \phi(\omega) + \omega\tau) \quad (2.13)$$

The phase difference between the two spectrally sheared replicas can be extracted algebraically using methods taken from Fourier Transform Spectral Interferometry (FTSI) [14]. The extraction of the phase difference $\phi(\omega+\delta\omega) - \phi(\omega) + \omega\tau$ is performed using a Fast Fourier Transform, a filtering of one of the interference terms, and a Fast Fourier Transform back to the initial experimental points.

A possible schematic of a SPIDER device is presented in Fig. 2.7. The pulse to be characterized is separated into two replicas with different intensities. The first arm (low intensity) is composed of an interferometer for producing and delaying two replicas by $\tau$. The second arm (high intensity) is constituted of a device for introducing a fixed amount of dispersion in order to stretch the pulse. The beams from the two arms are focused into a non linear crystal (BBO) for the sum frequency generation (SFG). The SPIDER signal is measured with a spectrometer.

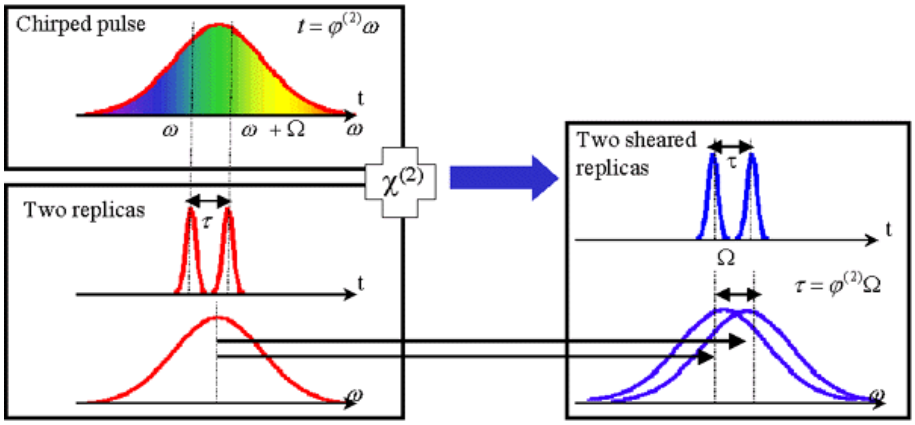


Figure 2.6: Generation of two sheared replicas of the input pulse by non-linear interaction with a chirped pulse. Reprinted from [3]

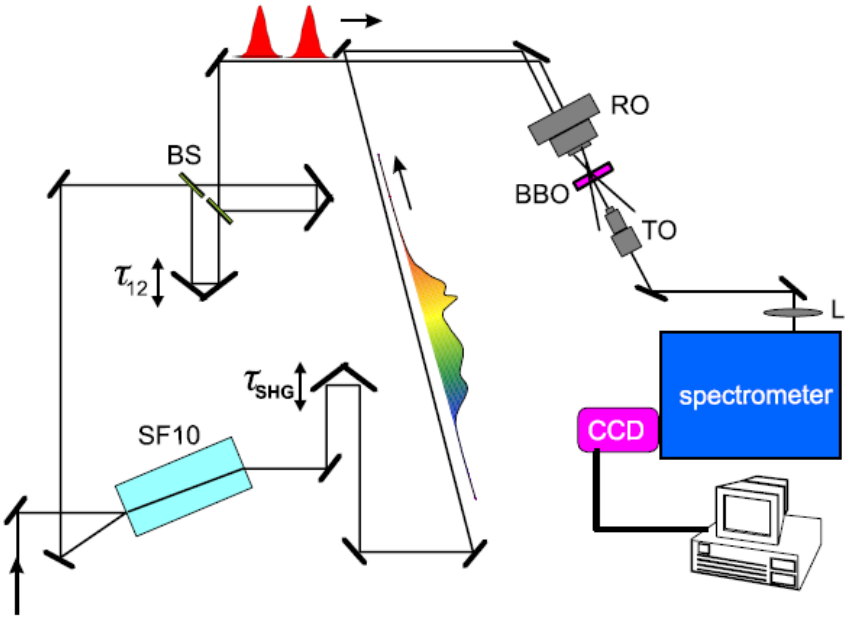


Figure 2.7: Example of SPIDER schematic. SF 10: glass block, BS: beam splitter, $\tau$: adjustable delay between unchirped replica, $\tau_{SHG}$: delay between unchirped pulses and strongly chirped pulse, RO: focusing lens, TO: collecting lens

### 2.3.3 FROG technique

Another technique for the complete pulse characterization is the FROG (Frequency Resolved Optical Gating) [8, 16]. This technique can be understood as a spectrally resolved autocorrelation. The result of the measurement is a time-frequency spectrogram and the spectral phase

and amplitude is extracted using an iterative algorithm. A schematic of a FROG device is shown in Fig. 2.8. The FROG measurement can use second or third order nonlinearity. The pulse to be measured with an electric field $E(t)$ interacts, in the non linear medium, with a temporal gate $G(t-\tau)$, being $\tau$ the delay between the pulses. The signal generated by the nonlinear interaction can be expressed as: $E_{signal}(t,\tau) = E(t)G(t-\tau)$. A spectrometer enables to measure the spectral intensity $I_{FROG}(\omega)$ for different delays $\tau$. The mathematical expression of the measured spectrogram is:

$$I_{FROG}(\omega,\tau) = \left| \int_{-\infty}^{+\infty} E(t)G(t-\tau)exp(-i\omega t)dt \right|^2 \tag{2.14}$$

Considering the case with SHG (non collinear geometry) as the nonlinear process, the gate function is the pulse to be measured delayed by $\tau$. The FROG trace (Fig. 2.9) can then be expressed as:

$$I^{SHG}_{FROG}(\omega,\tau) = \left| \int_{-\infty}^{+\infty} E(t)E(t-\tau)exp(-i\omega t)dt \right|^2 \tag{2.15}$$

With an iterative algorithm the spectral phase and amplitude is extracted from the trace.

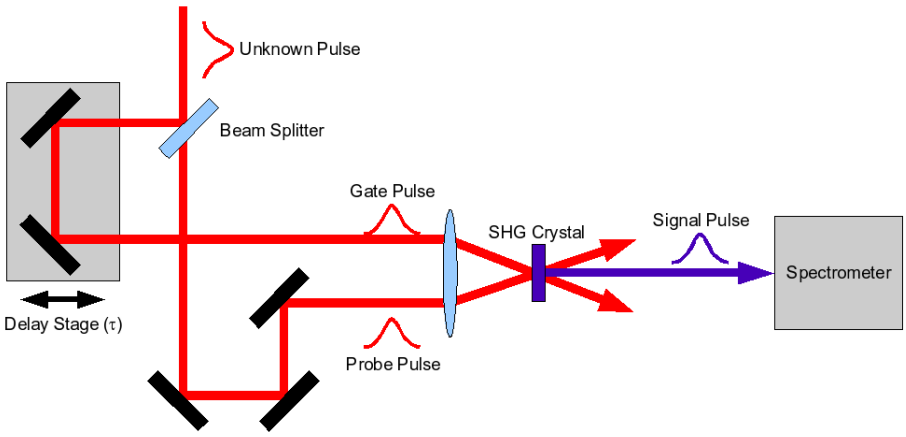


Figure 2.8: Schematic of a typical FROG (multishot SHG) setup.

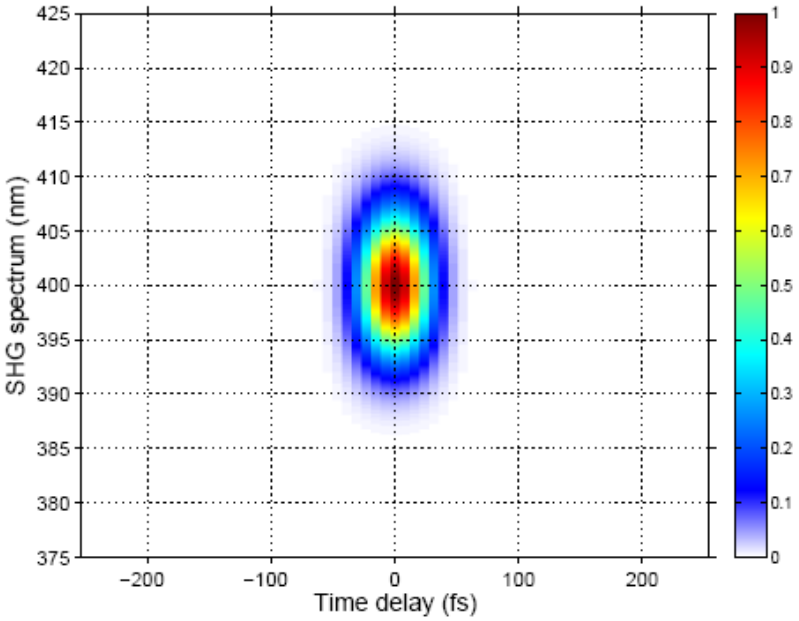


Figure 2.9: Example of a measured SHG FROG trace. The spectral phase and amplitude is extracted from this trace with an iterative algorithm

### 2.3.4 Phazzler

All the previous solutions for characterizing ultra-short pulses are made up by the same blocks. A linear interferometer, a non linear process and a detector. In particular it can be demonstrated that for the measurement of a pulse with an integrating detector (it is always the case for fs pulses) a non linear process is needed. As it will be shown in section 6.2.3, an Acousto-Optical Programmable Dispersive Filter (AOPDF, Dazzler) acts as a linear filter. In particular if $\left|\tilde{E}_{in}(\omega)\right|$ is the input spectral amplitude of an optical pulse, the spectral amplitude at the output of the programmable dispersive filter, $\left|\tilde{E}_{out}(\omega)\right|$, is equal to the product of $\left|\tilde{E}_{in}(\omega)\right|$ with the spectral transfer function $H(\omega)$:

$$\left|\tilde{E}_{out}(\omega)\right| = H(\omega)\left|\tilde{E}_{in}(\omega)\right| \tag{2.16}$$

The AOPDF can then substitute the linear interferometer of a pulse measurement device. This idea is implemented in the device for pulse shaping and characterization named Phazzler (Fastlite) [11] (Fig. 2.10). The main advantage of this solution is the extreme flexibility of the device: a FROG, a SPIDER and an autocorrelation measurement can be done with the same device without changing the elements inside and the alignment. Furthermore working in a collinear configuration makes the alignment extremely easy (there are two external pin-holes for the alinement). Generating two delayed replicas of the pulse with the pulse shaper opens also some new interesting features [10]. For example, scanning the delay between the two replicas can be realized, first, by shifting simultaneously the envelope and CEP as is the case for a mechanical delay line (for example moving one arm of a Michelson interferometer). In this case the spectral transfer function is $H(\omega) = exp(i(\omega - \omega_0)\tau)$, with $\omega_0$ the carrier frequency. We

define this optical delay. The second option is to shift only the envelope keeping the CEP fixed. In this case the spectral transfer function is $H(\omega) = exp(i(\omega\tau))$ and we define this pure delay. Any intermediate carrier envelope phase shift between the two extremes is also possible.

The spectral transfer function to produce to replicas delayed by $\tau$ (symmetric respect to t=0) is than given by the expression:

$$H(\omega) = \frac{1}{2}(exp(i(\omega - (1-\gamma)\omega_0))\tau/2 + exp(-i(\omega - (1-\gamma)\omega_0)\tau/2 \tag{2.17}$$

The CEP remains unchanged for $\gamma = 1$ (pure delay) and shifts together with the envelope for $\gamma = 0$ (optical delay).

When the two delayed pulses are generated for an interferometric autocorrelation measurement, changing the value of $\gamma$ changes the period of oscillation of the trace. In particular for $\gamma = 1$ the trace presents no oscillations and only the envelope is visible. This may seem surprising given the fact that the two wave propagate collinearly, but beautifully demonstrates the ability to control the CEP. This control of the CEP with the Dazzler will be discussed more precisely in section 6.9. When $\gamma = 1$ we define this as a base-band measurement. For $\gamma < 1$ oscillations appear and their periodicity can be adjusted at will through a choice of $\gamma$. While for $\gamma = 0$ the oscillation frequency matches the carrier frequency, for $\gamma = 0.5$ the oscillation frequency is reduced by a factor of two. For this reason this interferometric autocorrelation made with the Phazzler is called Pseudo Interferometric Autocorrelation (PIAC).

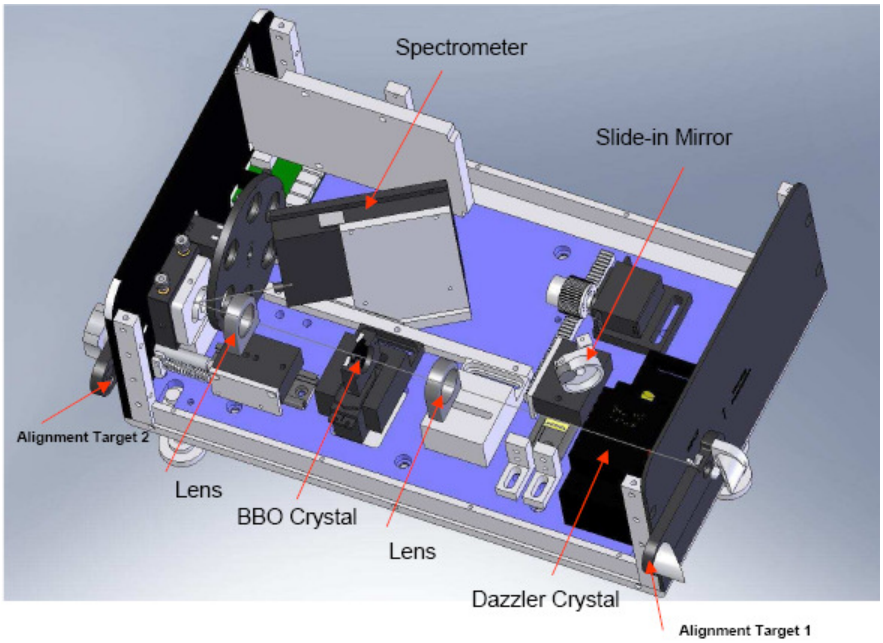


Figure 2.10: CAD drawing of the internal view of the Phazzler optical module. Reprinted from [11].

### Phazzler FROG

I have previously presented that a SHG FROG measurement is a frequency resolved interferometric autocorrelator. The expression for the FROG trace with collinear beams gives [13]:

$$I_{iFROG}^{SHG}(\omega,\tau) = \left| \int_{-\infty}^{+\infty} (E(t) + E(t-\tau))^2 exp(-i\omega t) dt \right|^2 \tag{2.18}$$

The Phazzler configuration for a FROG measurement is shown in Fig. 2.11. Changing the value of $\gamma$ affects the FROG trace. In particular when $\gamma = 1$ we obtain a baseband FROG trace (Fig. 2.12) and when $\gamma < 1$ an interferometric FROG trace (Fig. 2.13). As for a standard FROG, the spectral phase and amplitude are extracted from the FROG traces with an iterative algorithm.

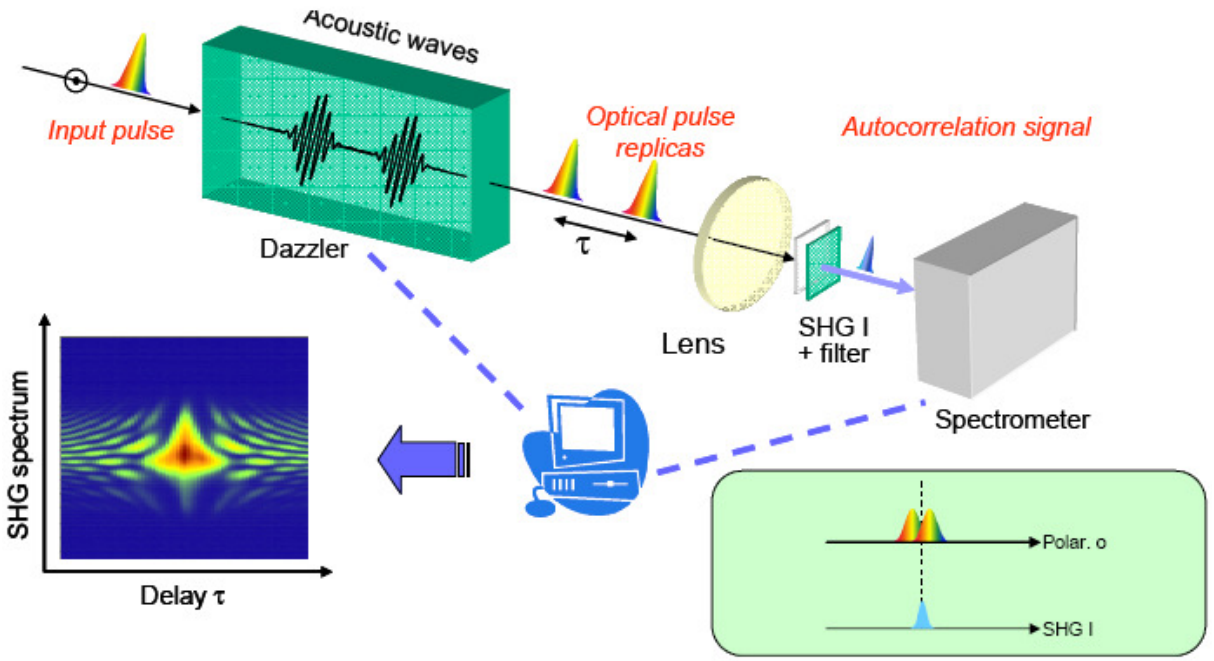


Figure 2.11: Schematic of a Phazzler FROG measurement

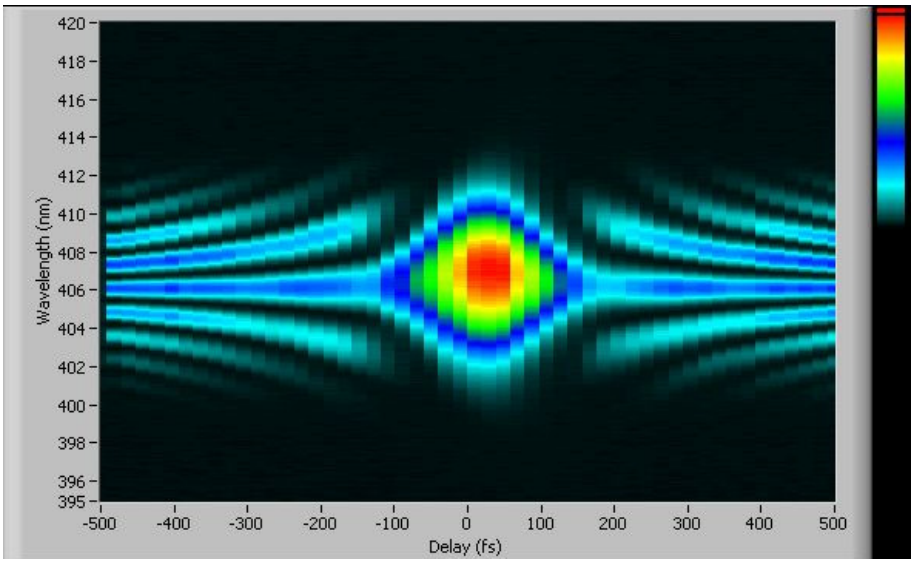


Figure 2.12: Experimental baseband ($\gamma = 1$) SHG FROG trace measured with the Phazzler. The pulse duration is 100 fs

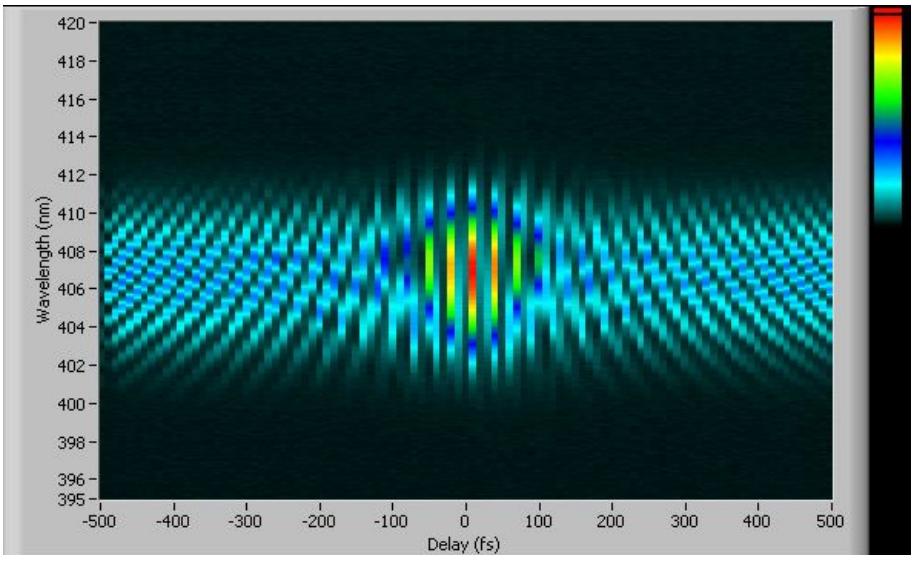


Figure 2.13: Experimental interferometric ($\gamma = 0.75$) SHG FROG trace measured with the Phazzler. The pulse duration is 100 fs

Until now I have only considered SHG FROG. Using this nonlinear effect has the drawback that there is an ambiguity in the temporal axis of the reconstructed temporal pulse and it is not possible to distinguish between the front and the back of the pulse. To avoid this ambiguity several third order non linear processes have been used (third harmonic generation, self diffraction, polarization gating...). XPW generation can also be a good candidate because it is a collinear process and the generated beam is easily separable from the fundamental using

a polarizer. As it will be clearly presented later, XPW generation has the other advantage of being achromatic and degenerate in wavelength. This means that the generated pulse is at the same wavelength as the fundamental. This is very important if we want to measure pulses in the UV where generating multiples of fundamental frequency (second, third harmonic generation) is not possible. The application of an XPW FROG for measuring UV pulses is one of the motivations for extending the study of the XPW process to shorter wavelengths(section 4.10). A Phazzler for measuring UV pulses using the XPW generation as a nonlinear process is under development. Fig. 2.14 shows an example of a baseband XPW FROG trace for a compressed pulse at 800 nm. The mathematical expression of the FROG trace in that case is given by:

$$I_{iFROG}^{XPW}(\omega,\tau) = \left| \int_{-\infty}^{+\infty} (E(t) + E(t-\tau))^3 exp(-i\omega t) dt \right|^2 \tag{2.19}$$

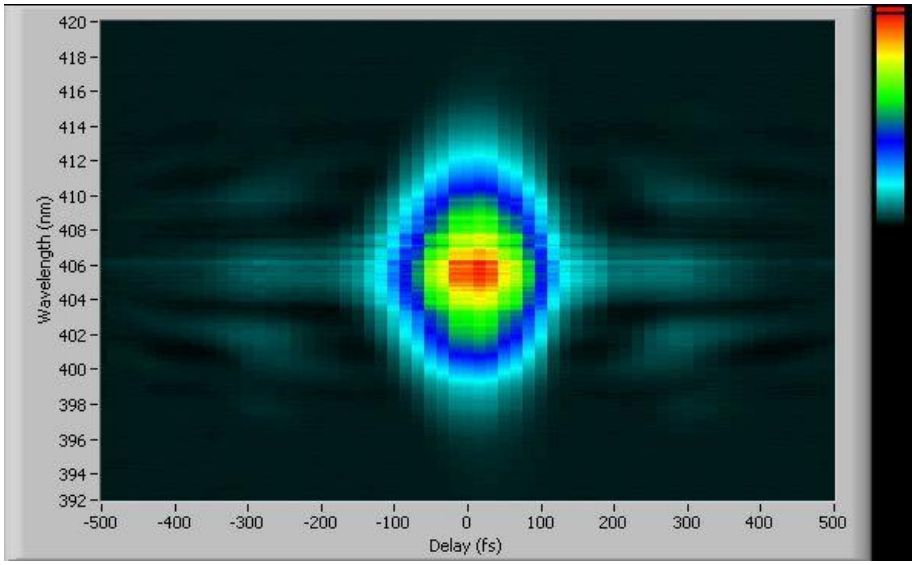


Figure 2.14: Experimental baseband ($\gamma = 0$) XPW FROG trace measured with the Phazzler

### Phazzler SPIDER

Working with a pulse shaper as a substitute for the linear interferometer has several advantages also concerning the SPIDER measurement. The technique can be made totally collinear, the interpulse delay is accurately known (without any need for external calibration), the spectral shear is also known with an accuracy equal to the spectral resolution of the pulse shaper and all the parameters can be changed at will. When a type I SHG crystal is used this measurement is called a phase cycling SPIDER (cSPIDER). This variant is multi-shot (as it will be clear later 4 shots are needed for the reconstruction) but the optical setup is single beam and reduced to the same number of elements : the AOPDF, a type I SHG crystal and the spectrometer.
In this variant of the SPIDER there is a combination of three collinear pulses in the same

polarization state: two well separated time-delayed replicas $(E(t-\tau/2), E(t+\tau/2))$ and one chirped pulse with the time-dependent complex envelope $F(t)$:

$$E_{++}(t) = E(t-\tau/2) + E(t+\tau/2) + F(t) \tag{2.20}$$

In time domain and for perfect phase matching over the full spectrum, the type I SHG signal is proportional to the square of $E_{++}(t)$. If the interpulse delay $\tau$ is much larger than the pulse duration, the cross-terms between the pulse replicas vanishes and the only remaining cross-term corresponds to the SPIDER signal. Unfortunately, the only physical quantity experimentally accessible is the spectral intensity of the SHG spectrum $I_{++}(\omega)$, that is the square modulus of the Fourier Transform of $E^2_{++}(t)$. As a result, the experimental signal contains several parasitic signals together with the SPIDER signal. Phase cycling can be used to eliminate the parasitic terms by linear combination of several measurements. More precisely, given the SHG signals of the four following pulse combinations (obtained by changing the sign of the transfer function of the AOPDF):

$$E_{++}(t) = \pm E(t-\tau/2) \pm E(t+\tau/2) + F(t) \tag{2.21}$$

the SPIDER signal is extracted by the following combination:

$$I_{SPIDER}(\omega) = I_{++}(\omega) + I_{++}(\omega) - I_{+-}(\omega) - I_{-+}(\omega) \tag{2.22}$$

The input spectral phase is retrieved from this SPIDER signal with the same method presented in section 2.3.2.

### 2.3.5 Third order correlator

In section 2.2.2 I showed that to characterize the temporal quality of a femtosecond pulse it is not sufficient to measure its temporal duration but also its temporal contrast. The device used to measure this temporal contrast with a high dynamic range (>10 orders of magnitude) is a third order correlator. The schematic of this measurement is shown in Fig. 2.15. In this device the beam passes thought a variable attenuator and is then separated into two different paths. In the first the beam is frequency doubled. In the other the fundamental beam passes through a motorized delay line. The fundamental and the second harmonic interact in a BBO crystal for the generation of the third harmonic by sum frequency generation. The third harmonic is then separated from the other pulses and is detected with a photomultiplier. The third order correlation signal is given by the expression:

$$S_{3\omega}(\tau) = \int_{-\infty}^{+\infty} I_{2\omega}(t) I_{\omega}(t-\tau) dt \tag{2.23}$$

The temporal contrast of the input beam is estimated by measuring the temporal contrast of the correlation trace. This trace has a high temporal dynamic because the parasitic sources of third harmonic are limited to the third harmonic generation generated directly by the fundamental beam.

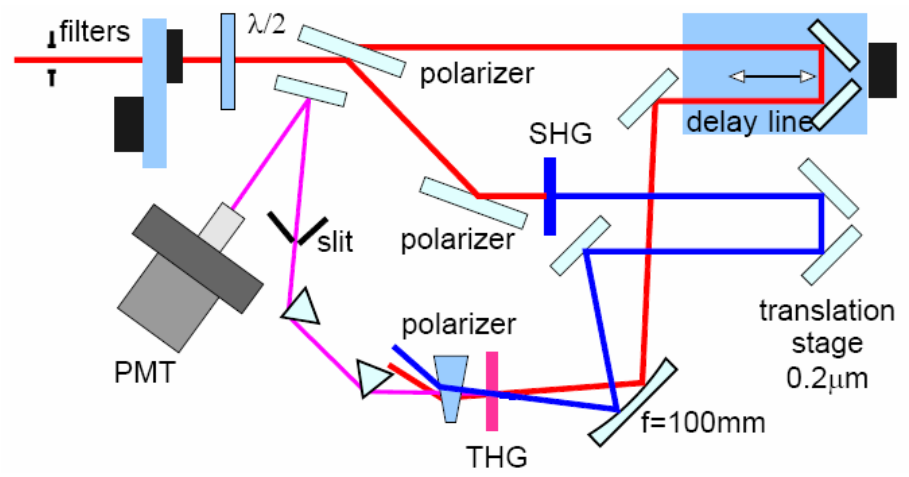


Figure 2.15: Schematic for a high dynamic third order correlator

# Bibliography

[1] A. Apolonski, A. Poppe, G. Tempea, Ch. Spielmann, Th. Udem, R. Holzwarth, T. W. Hänsch, and F. Krausz. Controlling the phase evolution of few-cycle light pulses. *Phys. Rev. Lett.*, 85(4):740–743, 2000.

[2] J-C. M. Diels, J. J. Fontaine, I. C. McMichael, and F. Simoni. Control and measurement of ultrashort pulse shapes (in amplitude and phase) with femtosecond accuracy. *Appl. Opt.*, 24(9):1270–1282, 1985.

[3] http:ultrafast.physics.ox.ac.uk.

[4] http:nanooptics.uni-graz.at

[5] C. Iaconis and I. A. Walmsley. Spectral phase interferometry for direct electric-field reconstruction of ultrashort optical pulses. *Opt. Lett.*, 23(10):792–794, 1998.

[6] C. Iaconis and I. A. Walmsley. Self-referencing spectral interferometry for measuring ultrashort optical pulses. *IEEE J. Quantum Electron.*, 35(4):501–509, 1999.

[7] M. Kaluza, J. Schreiber, M. I. K. Santala, G. D. Tsakiris, K. Eidmann, J. Meyer-ter Vehn, and K. J. Witte. Influence of the laser prepulse on proton acceleration in thin-foil experiments. *Phys. Rev. Lett.*, 93(4):045003–, July 2004.

[8] D. J. Kane. Single-shot measurement of the intensity and phase of an arbitrary ultrashort pulse by using frequency-resolved optical gating. *Opt. Lett.*, 18(10):23–25, 1993.

[9] X. Liu, R. Wagner, A. Maksimchuk, E. Goodman, J. Workman, D. Umstadter, and A. Migus. Nonlinear temporal diffraction and frequency shifts resulting from pulse shaping in chirped-pulse amplification systems. *Opt. Lett.*, 20(10):1163–1165, 1995.

[10] T. Oksenhendler PhD manuscript.

[11] Phazzler manual.

[12] Y. Nomura PhD manuscript.

[13] G. Stibenz and G. Steinmeyer. Interferometric frequency-resolved optical gating. *Opt. Express*, 13(7):2617–2626, 2005.

[14] M. Takeda, H. Ina, and S. Kobayashi. Fourier-transform method of fringe-pattern analysis for computer-based topography and interferometry. *J. Opt. Soc. Am.*, 72(1):156–160, 1982.

[15] C. Thaury, F. Quere, J.-P. Geindre, A. Levy, T. Ceccotti, P. Monot, M. Bougeard, F. Reau, P. d'Oliveira, P. Audebert, R. Marjoribanks, and Ph. Martin. Plasma mirrors for ultrahigh-intensity optics. *Nat Phys*, 3(6):424–429, June 2007.

[16] R. Trebino, A. Baltuska, M. S. Pshenichnikov, and D. A. Wiersma. *Few-Cycle Laser Pulse Generation and Its Applications*, volume 95, chapter Measuring Ultrashort Pulses in the Single-Cycle Regime: Frequency-Resolved Optical Gating, pages 231–264. Springer-Verlag, 2004.

[17] M. Zepf, G. D. Tsakiris, G. Pretzler, I. Watts, D. M. Chambers, P. A. Norreys, U. Andiel, A. E. Dangor, K. Eidmann, C. Gahn, A. Machacek, J. S. Wark, and K. Witte. Role of the plasma scale length in the harmonic generation from solid targets. *Phys. Rev. E*, 58(5):R5253–R5256, Nov 1998.